

Synthesis of controlled-size starch nanoparticles and superparamagnetic starch nanocomposites by microemulsion method

Diana Morán^{a,b}, Gemma Gutiérrez^{a,b}, Rafael Mendoza^c, Marilyn Rayner^d, Carmen Blanco-López^{b,c}, and María Matos^{a*,b}

^a *Department of Chemical and Environmental Engineering, University of Oviedo, Julián Clavería 8, 33006 Oviedo, Spain*

^b *Instituto Universitario de Biotecnología de Asturias, University of Oviedo, 33006 Oviedo, Spain*

^c *Department of Physical and Analytical Chemistry, University of Oviedo, Julián Clavería 8, 33006 Oviedo, Spain*

^d *Department of Food Technology, Engineering, and Nutrition, Lund University, P.O. Box 124, SE 221 00 Lund, Sweden*

*Corresponding author at: Department of Chemical and Environmental Engineering, University of Oviedo, Julián Clavería 8, 33006, Oviedo, Spain. Tel: +34 985 103029; Fax: +34 985 103434
E-mail addresses: matosmaria@uniovi.es, mariamatos@fq.uniovi.es (M. Matos).

Abstract

In this study, a synthesis process based on the microemulsion method (ME) was developed with the aim to produce controlled-size starch nanoparticles (SNPs). Several formulations were tested for the preparation of the W/O microemulsions varying the organic/aqueous phase ratios and co-stabilizers concentrations. SNPs were characterized in terms of size, morphology, monodispersity and crystallinity. Spherical shape particles with mean sizes 30-40 nm were prepared.

The method was then used to simultaneously synthesize SNPs and iron oxide nanoparticles with superparamagnetic properties. Starch-based nanocomposites with superparamagnetic properties and controlled size were obtained. Therefore, the microemulsion method developed could be considered an innovative technology for the design and development of novel functional nanomaterials. The starch-based nanocomposites were evaluated in terms of morphology and magnetic properties, and they are being considered as promising sustainable nanomaterials for different biomedical applications.

Keywords

Starch nanoparticles, microemulsion, size control, superparamagnetic particles, nanocomposites

Chemical compounds studied in this article

Sodium hydroxide (PubChem CID: 14798); Urea (PubChem CID: 1176); Absolute ethanol (PubChem CID: 702); CTAB (PubChem CID: 5974); 1-Butanol (PubChem CID: 263); 1-Hexanol (PubChem CID: 8103); Ammonia (PubChem CID: 222); Ferric chloride hexahydrate (PubChem CID: 16211236); Ferrous chloride tetrahydrate (PubChem CID: 16211588); Hydrochloric acid (PubChem CID: 313).

36 **1. Introduction**

37 Starch is a natural, renewable, biodegradable, and biocompatible polysaccharide and it is the main
38 source of carbohydrate storage in plants (Liu, Li, Li, Zhang & Li, 2021). From the chemical point of
39 view, it is a polymer composed by two polysaccharides, amylose and amylopectin, both made up of by
40 glucose units. Starch nanoparticles (SNPs) are considered one of the most promising novel sustainable
41 biomaterials for use in many different biotechnological applications. SNPs are obtained from starch
42 granules through different physical and chemical techniques and both the synthesis method and the
43 operating conditions influence their final properties for different further applications.

44 Several physicochemical methods have been reported to produce SNPs. Some of them are high-pressure
45 nanoemulsification, crosslinking, microemulsion or nanoprecipitation, among others (Kim, Park & Lim,
46 2015; Le Corre, Bras & Dufresne, 2010; Saari, Fuentes, Sjö, Rayner & Wahlgren, 2017; Chin, Azman
47 & Pang, 2014; Chin, Pang & Tay, 2011; Najafi, Baghaie & Ashori, 2016; Morán et al, 2021). The
48 microemulsion method is a soft chemistry technique with a growing interest is a soft chemistry
49 alternative with a growing interest as it does not require sophisticated equipment, hazardous reagents or
50 extreme conditions. Moreover, efficient control of the size, shape, monodispersity and composition of
51 SNPs can be achieved (Chin et al., 2014). Microemulsions are an alternative and novel approach for the
52 SNPs synthesis, as their composition and structure can be optimized to achieve the desired
53 characteristics of the SNPs (Asgari, Saberi, McClements & Lin, 2019). Water-in-oil (W/O)
54 microemulsions consist of small water droplets (dispersed or internal phase) dispersed in an oily phase
55 (continuous, external or dispersing phase), where surfactants and co-surfactants are present to stabilize
56 the interphase. The small water domains formed within the microemulsions can be used as nanoreactors
57 where the starch precipitates as SNPs (Asgari et al., 2019).

58 Nanotechnology is opening new horizons at the biomedical field and optical, electronic, chemical and
59 mechanical applications (Darroudi, Hakimi, Goodarzi & Kazemi Oskuee, 2014). Magnetic
60 nanoparticles have been studied for drug delivery, enzyme immobilization (Vaghari et al., 2016) and
61 different biotechnological purposes (Materón et al., 2021). They are composed of pure metals, metal
62 alloys and metal oxides (Malhotra et al. 2020). Iron oxide nanoparticles (IONPs), in particular, are
63 frequently used due their minimal toxicity and excellent physico-chemical properties such as the
64 superparamagnetism, and their biocompatibility and stability in aqueous solutions (Medeiros et al.,
65 2015; Soares et al., 2016; Valdiglesias et al., 2016). The feasibility of producing loaded magnetic iron
66 oxide-impregnated SNPs by a synthesis based on an emulsion crosslinking method has been reported.
67 These nanocomposites are attractive as possible and potential drug carriers for magnetically directed
68 drug delivery (Likhitar & Bajpai, 2012).

69 Our research group has developed a microemulsion method to produce size-tuned iron oxide
70 nanoparticles with superparamagnetic properties (Salvador et al., 2021). In the present study, the main
71 objective was to adapt and optimize this microemulsion method to produce controlled-size SNPs, and
72 then use it to carry out the simultaneous synthesis of both types of nanoparticles (SNPs and IONPs).

73 Thus, one of the most remarkable research advances of this work is to demonstrate the versatility of
74 using the microemulsion method to synthesize sustainable nanoparticles of different nature with slight
75 modifications in the W/O microemulsion formulation prepared for this purpose, and also the ability to
76 nanoprecipitate them simultaneously. Therefore, the hypothesis of this study is that by optimizing the
77 formulation of the W/O microemulsion used for the precipitation of nanoparticles, as well as the
78 formulation of the precipitating agent, it is possible to simultaneously synthesize controlled-size starch
79 nanoparticles and iron oxide nanoparticles with superparamagnetic properties to develop sustainable
80 novel nanocomposites, which will demonstrate that the proposed ME method is an innovative
81 technology for the design and development of new and novel nanomaterials.

82 Thus, in this work, controlled-size SNPs were synthesized by the W/O ME method using different
83 formulations for the microemulsions preparation and optimizing the proportion and composition of the
84 aqueous phase, the organic phase and the amounts of stabilizer, co-stabilizer, and the type of
85 precipitating agents used. The synthesized SNPs were characterized in terms of shape and size by
86 dynamic light scattering (DLS) (Nanozetasizer from Malvern) and scanning electronic microscopy
87 (SEM). X-ray powder diffraction (XRPD) was used to analyze the crystallinity of both the granules and
88 resulting SNPs. Nanocomposites of SNPs and IONPs have been synthesized by the ME method, and
89 their morphology and magnetic properties have been studied.

90

91 **2. Materials and methods**

92 **2.1. Materials**

93 Cetyl Trimethyl Ammonium Bromide 99 % (CTAB, $C_{19}H_{42}BrN$, $M_w = 364.46$ g/mol), was supplied as
94 a white powder by Sigma-Aldrich (USA). This is a quaternary ammonium salt, with long alkyl and
95 detergent activity. In this cationic surfactant, the hydrophilic part is positively charged, and its
96 hydrophilic-lipophilic balance (HLB) value is 10. 1-Butanol was supplied by Sigma Aldrich (USA) and
97 was used as a co-stabilizer in the microemulsion. 1-Hexanol, supplied by Alfa Aesar (USA), acts as the
98 organic phase in the microemulsion as it has a longer alkyl chain than that of 1-butanol.

99 Milli-Q water was used to prepare the solutions to be used in the synthesis and for the subsequent
100 washing of the nanoparticles. Absolute ethanol supplied by Sigma Aldrich (USA) was also used to wash
101 the nanoparticles.

102 Maize starch with 0.25% moisture and a branching (α -1,4)/(α -1,6) ratio of 15.2 was purchased from
103 Cerestar-AKV I/S (Denmark). It was presented as a white powder insoluble in water at room
104 temperature.

105 NaOH ($M_w = 39.997$ g/mol) was supplied by Panreac AppliChem (Spain) and used was used as a
106 precipitating agent for the SNPs synthesis, as well as for the formulation of the aqueous phases. Urea
107 ($M_w = 60.056$ g/mol), was supplied by Serva Electrophoresis GmbH (Germany). This reagent is
108 presented as white crystalline powder and due to its dipole moment, it is soluble in water and in alcohol.
109 In this work it was also used for the formulation of the aqueous phases.

110 Ammonia 30% (NH_3 , $M_w = 17.03$ g/mol) was used as a precipitating agent in order to alkalinize the
111 aqueous solution containing the starch and the iron salts and precipitate them in the form of
112 nanoparticles. It was provided by Panreac AppliChem (Spain). Ferric chloride hexahydrate ($\text{FeCl}_3 \cdot 6$
113 H_2O , $M_w = 270.30$ g/mol), a very hygroscopic yellow-orange crystalline solid, was supplied by Panreac
114 AppliChem (Spain). Ferrous chloride tetrahydrate ($\text{FeCl}_2 \cdot 4 \text{H}_2\text{O}$, $M_w = 198.81$ g/mol) was supplied by
115 J.T. Baker (USA). It is a light green solid, soluble in water and with a high tendency to oxidize to ferric
116 chloride. Both the ferric and the ferrous chloride were used in an aqueous solution as precursors for the
117 production of magnetite. Hydrochloric acid 38% (HCl), was supplied by Sigma-Aldrich (Germany) and
118 it was used to prepare the aqueous solution of iron salts.

119 **2.2. Methods**

120 Microemulsion (ME) method was adapted from a previous works for synthesis of superparamagnetic
121 nanoparticles (Salvador et al., 2021). The obtention of the SNPs by this ME method can be achieved in two
122 steps: (i) preparation of the microemulsion systems and (ii) synthesis of the SNPs by adding the
123 precipitating agent.

124 **2.2.1. Preparation of the microemulsions**

125 Microemulsions formulated in this work were W/O type, i.e., water droplets dispersed into an oily phase.
126 To obtain a W/O microemulsion, the oily phase contained the organic solvent, alcohol as co-stabilizer
127 and surfactant as stabilizer. The surfactant and alcohol molecules are arranged as reverse micelles, which
128 means that the water-soluble hydrophilic heads point towards the inner part of the droplets, while the
129 hydrophobic tails point towards the outside, where the organic solvent is found.

130 Subsequently, this organic phase was in contact with an aqueous phase in which the biopolymer was
131 dissolved, and this quickly diffused towards the hydrophilic regions of the micelles, giving rise to the
132 formation of nanometric hydrophilic regions rich in biopolymer, with diameters generally less than 100
133 nm. These small water regions that will later act as templates for the SNPs formation can be called
134 nanoreactors (Asgari et al., 2019).

135 To obtain the microemulsions, a series of steps must be followed, as detailed below.

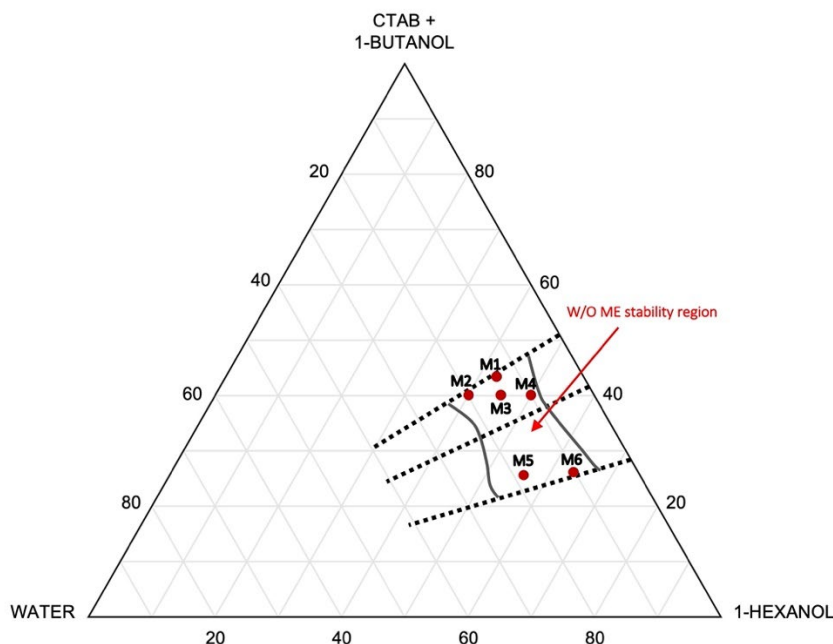
136 **2.2.1.1. Preparation of the aqueous phase**

137 First, 1% (w/v) starch solution was prepared by dissolving 0.2 g of starch into 20 mL of a solvent system.
138 Three different solvents were tested: (i) Milli-Q water, (ii) 8% (w/v) NaOH, and (iii) 8% (w/v) NaOH +
139 10% (w/v) urea. This starch solution was kept under a 1000 rpm constant stirring at 80°C for 30 min
140 until the starch was fully dissolved, obtaining a completely homogeneous solution. These synthesis
141 parameters were selected based on a previous work (Gutiérrez et al., 2020).

142 **2.2.1.2. Microemulsions formulation**

143 In order to formulate the microemulsions, an organic solution consisting of a mixture of CTAB
144 (surfactant that acts as a stabilizer), 1-butanol (co-stabilizer) and 1-hexanol (organic phase) was
145 prepared. A 3:2 mass ratio of surfactant to co-stabilizer was kept constant in all formulations. 1-butanol
146 is distributed mainly between the interfacial layer and the organic phase, acting as a co-stabilizer in the

147 interfacial layer and as a co-solvent in the organic phase (Wang, Chen, Luo, Fu, 2016).
 148 Different microemulsion formulations were studied. In order to determine the appropriate composition
 149 for SNPs preparation, a microemulsion stability region must first be determined by the titration method
 150 in a ternary diagram (Salvador et al., 2021). Figure 1 shows the six optimal microemulsion formulations
 151 selected from previous studies for the present work (M1, M2, M3, M4, M5 and M6).



152
 153 *Figure 1. Ternary diagram of the CTAB-butanol-hexanol-water system with the composition of the*
 154 *microemulsions studied for the SNPs synthesis (M1 to M6).*
 155

156 Once the six best formulations for obtaining the microemulsions were identified, the surfactant and the
 157 co-stabilizer were added to the organic phase by weighing. Subsequently, this mixture was kept under
 158 high agitation for 10 min until a homogeneous solution was obtained. Afterwards, the aqueous phase
 159 prepared above was added, and the mixture was gently stirred to promote homogenization and hence
 160 microemulsion formation. Due to the small size of the aqueous droplets formed (values less than 1
 161 micron), light can pass through them, so microemulsion formation was evident once the solution became
 162 totally translucent. Table 1 gathers the compositions of the different reagents of each microemulsion
 163 formulation.

164
 165 *Table 1. Microemulsion composition of the six formulations selected within the microemulsion stability*
 166 *region for the SNPs synthesis.*

Microemulsion system	Microemulsion composition (g)			
	CTAB	1-Butanol	1-Hexanol	Aqueous phase
M1	5	4	9	3
M2	5	3	8	4
M3	5	3	9	3

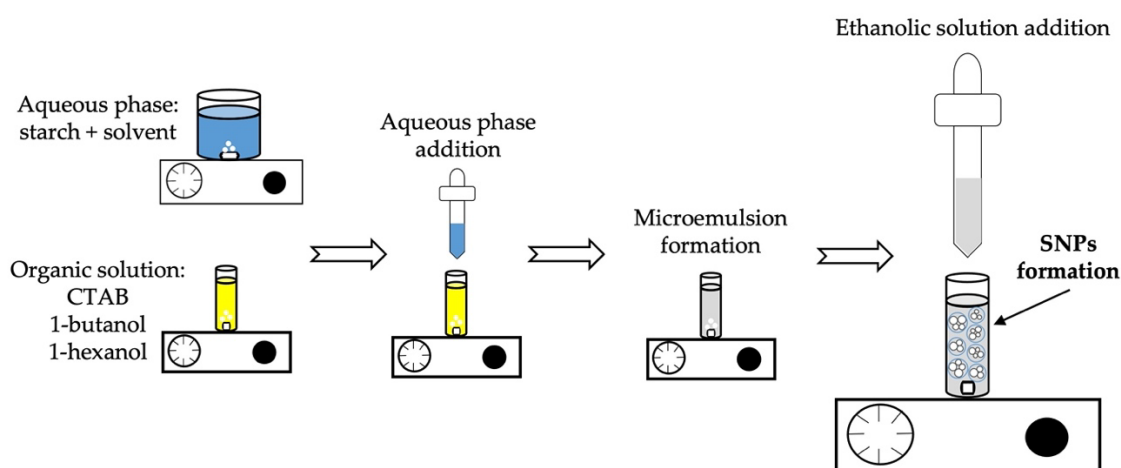
M4			10	2
M5	3	2	11	4
M6			13	2

167

168 2.2.2. Synthesis of the SNPs

169 SNPs were obtained by adding a solution containing a precipitating agent (an organic solvent) to the
 170 previously prepared microemulsion which causes the starch to precipitate in the form of nanoparticles
 171 inside the water droplets of the microemulsion. Two precipitating agents were tested: (i) 12% (w/v)
 172 NaOH + ethanol, and (ii) pure ethanol. For the preparation of the NaOH solution, it was necessary to
 173 stir the mixture at 500 rpm for 24 h at room temperature due to the low solubility of NaOH in ethanol
 174 with respect to its solubility in water.

175 Once the precipitating solution was ready, it was added dropwise to the microemulsion system, keeping
 176 the mixture under constant high stirring at all times. SNPs formation was noted visually as small white
 177 aggregates appeared in the solution as drops were added. As soon as these aggregates appeared, the
 178 addition of the drops was stopped since the SNPs were formed. A scheme of this process is shown at
 179 Figure 2.



180

181 *Figure 2. Scheme of the SNPs synthesis process by the microemulsion method.*

182

183 Once the SNPs were obtained and prior to their characterization, samples had to be carefully washed to
 184 remove the excess of stabilizers or solvents. First, samples were centrifuged at room temperature for 10
 185 min at 10000 rpm and the supernatant was removed to obtain the particles as pellets, which were then
 186 washed six times with alternate washes of ethanol and 50%-50% mixtures of absolute ethanol and Milli-
 187 Q water, centrifuging again under the same conditions between each washing step.

188 2.2.3. Synthesis of the starch superparamagnetic nanocomposites

189 The same microemulsion method was followed for the obtention of composites SNPs-IONPs. However,
 190 in this case, the aqueous phase consisted of a mixture of solutions of starch and iron salts. A 2.5% (w/v)
 191 starch solution was prepared by dissolving 0.5 g of starch into 20 mL of Milli-Q water under 1000 rpm
 192 constant stirring at 80°C for 30 min. In turn, a 50 mL solution with a molar ratio of iron salts Fe^{2+}/Fe^{3+}

193 of 0.5 was prepared, containing 0.01 M of HCl to prevent further oxidation of the Fe²⁺. When both
194 solutions were completely dissolved, they were mixed and kept at 1000 rpm constant stirring at 80°C
195 for 30 min. Once prepared, the final solution was allowed to cool until room temperature was reached.
196 Finally, it was added to the CTAB-1-butanol-1-hexanol system to form the microemulsion, as for the
197 SNPs synthesis. The same 6 microemulsion systems were also studied in this case.

198 The SNP-IONPs composites were achieved by adding the precipitating agent (30% (v/v) ammonia
199 solution) dropwise to the microemulsion under high stirring. The synthesis of the nanoparticles was now
200 visually detected by the appearance of a mixture of a black precipitate and white nanoparticles.
201 Therefore, at that moment, the addition of ammonia was stopped. The solution was left under magnetic
202 stirring for 2 h and then washed several times with distilled water assisted by a permanent magnet.

203 **2.3. SNPs characterization**

204 **2.3.1. Particle size distribution**

205 An approximate idea of the hydrodynamic size (in number) and the homogeneity (PDI) of the particles
206 was obtained by dynamic light scattering (DLS) using a Zetasizer Nano ZS equipment (Malvern
207 Instruments Ltd, Malvern, UK). Samples were measured with the 173° backscatter detector in low
208 volume disposable cuvettes (Malvern Instruments Ltd, Malvern, UK).

209 **2.3.2. Morphology and size**

210 The final size and shape of the SNPs were analyzed using a JEOL JSM-5600 field emission scanning
211 electron microscope at an acceleration voltage of 20 kV. Samples were dried in a stove for 24 h at 80°C.
212 Once dehydrated, they were fractured with a spatula and deposited on a double-sided adhesive tape on
213 a copper substrate. They were coated with a gold thin film in Balzers SCD 005 sputtering device (Bal-
214 Tec AG, Liechtenstein) prior to the analysis to prevent the electric charge built-up under the electron
215 beam in the microscope. The average particle size of the SNPs was determined by random measurements
216 on the images using ImageJ software.

217 Furthermore, the final size and shape of the superparamagnetic SNPs were analyzed using a transmission
218 electron microscope (TEM JEOL-2000 EX-II). An aliquot of an aqueous suspension of the samples was
219 placed into a copper-grid supported transparent carbon foil and analyzed. The average particle size was
220 also determined by using ImageJ software.

221 **2.3.3. X-ray powder diffraction (XRPD) analysis**

222 X-ray powder diffraction (XRPD) was used to determine the crystalline structure of the synthesized
223 SNPs as well as the starch granules. The powder X-ray diffraction data for the samples were collected
224 at RT, using CuK α 1.2 radiation ($\lambda = 1.54056 \text{ \AA}$ and 1.54439 \AA) in a Bragg-Brentano reflection
225 configuration, on a Philips Panalytical X'Pert Pro diffractometer in a 2θ range of 5-27°, with a step size
226 of 0.08356. The estimation of the crystalline domain sizes of the SNPs was obtained using the FullProf
227 program.

228 **2.3.4. Magnetic characterization**

229 An EV9 vibrating sample magnetometer (VSM) equipped with an electromagnet producing fields up to

230 ± 2.2 T was used to obtain the magnetization curves of the superparamagnetic SNPs and IONPs at room
 231 temperature (298.15 K). Powder samples were analyzed, by using 0.05 T field steps, and the results were
 232 normalized to the magnetic phase.

233 3. Results and discussion

234 3.1. Starch nanoparticles (SNPs)

235 3.1.1. Particle size distribution, size and morphology

236 As explained in sections 2.2.1 and 2.2.2, the synthesis of the SNPs was carried out under different
 237 synthesis conditions, studying different microemulsion systems (M1 to M6) and different ethanolic
 238 solutions. The purpose was to optimize the method and to achieve the precipitation of the starch in the
 239 form of nanoparticles.

240 Results for the morphological characterization for each system are shown at Table 2. The particle size
 241 distributions and the polydispersity indices (PdI) were obtained by DLS, and the shape of the particles
 242 (spherical or non-spherical) by SEM.

243 The protocol was the same for each case: first SNPs were synthesized (different compositions), after the
 244 washing steps, they were characterized by DLS and finally, they were dried and characterized by SEM.

245 All the experiments were performed in triplicate (at least) in order to evaluate their reproducibility.

246

247 *Table 2. Main sizes of SNPs obtained by the microemulsion method with the different microemulsion*
 248 *systems studied*

Sample	Aqueous phase (%w/v)	Precipitating agent (%w/v)	Size (nm)	PdI	Spherical shape
M1-A	Starch + Milli-Q	NaOH 12% + ethanol	165±19	0.75±0.0	Yes
M1-B	Starch + Milli-Q	Ethanol	- ¹	- ¹	- ¹
M1-C	Starch + NaOH 8%	Ethanol	21±3	0.49±0.0	No
M1-D	Starch + NaOH 8% + urea	Ethanol	43±5	0.60±0.0	No
M2-A	Starch + Milli-Q	NaOH 12% + ethanol	40±3	0.81±0.1	Yes
M2-B	Starch + Milli-Q	Ethanol	- ¹	- ¹	- ¹
M2-C	Starch + NaOH 8%	Ethanol	29±4	0.27±0.0	No
M2-D	Starch + NaOH 8% + urea	Ethanol	43±10	0.55±0.0	No
M3-A	Starch + Milli-Q	NaOH 12% + ethanol	34±10	0.77±0.1	Yes
M3-B	Starch + Milli-Q	Ethanol	- ¹	- ¹	- ¹
M3-C	Starch + NaOH 8%	Ethanol	31±4	0.54±0.1	Yes
M3-D	Starch + NaOH 8% + urea	Ethanol	38±6	0.55±0.0	No
M4-A	Starch + Milli-Q	NaOH 12% + ethanol	- ¹	- ¹	- ¹
M4-B	Starch + Milli-Q	Ethanol	- ¹	- ¹	- ¹
M4-C	Starch + NaOH 8%	Ethanol	28±5	0.48±0.0	No
M4-D	Starch + NaOH 8% + urea	Ethanol	48±3	0.58±0.1	Yes
M5-A	Starch + Milli-Q	NaOH 12% + ethanol	36±7	0.98±0.0	Yes

M5-B	Starch + Milli-Q	Ethanol	- ¹	- ¹	- ¹
M5-C	Starch + NaOH 8%	Ethanol	66±13	0.47±0.0	Yes
M5-D	Starch + NaOH 8% + urea	Ethanol	47±4	0.61±0.0	Yes
M6-A	Starch + Milli-Q	NaOH 12% + ethanol	40±4	0.64±0.1	Yes
M6-B	Starch + Milli-Q	Ethanol	- ¹	- ¹	- ¹
M6-C	Starch + NaOH 8%	Ethanol	24±3	0.42±0.0	Yes
M6-D	Starch + NaOH 8% + urea	Ethanol	58±17	0.52±0.0	No

249 ¹ No DLS available.

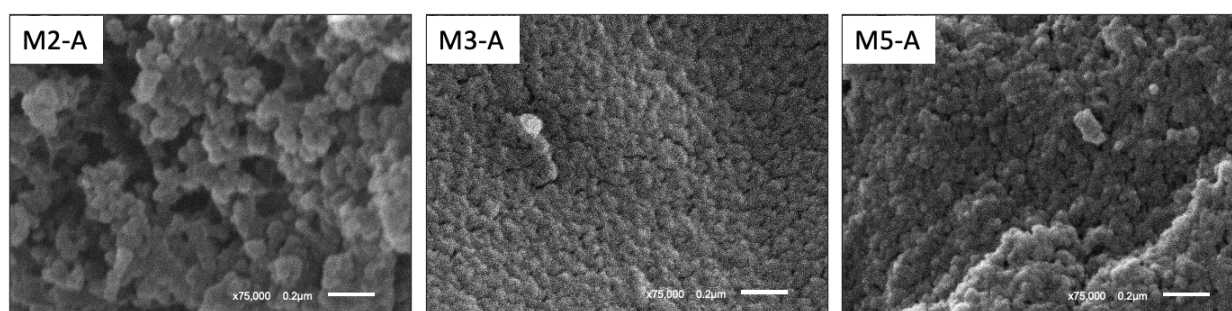
250

251 Looking at the DLS size results in Table 2, a first conclusion can be reached: the smallest particle sizes
252 were reached when NaOH was present in the aqueous phase, obtaining relatively small sizes both in
253 presence and absence of urea (samples C and D of each system) in most of the cases studied. For each
254 formulation tested, particle sizes were smaller in the absence of urea, except for the M5 microemulsion
255 system where the smallest sizes were obtained when both NaOH and urea were present in the aqueous
256 phase with the starch. However, when samples were analyzed by SEM, only five of them presented a
257 spherical shape (M3-C, M4-D, M5-C, M5-D and M6-C) but most of them shown agglomerates.

258 When NaOH acted as the precipitating agent (sample A of each system), small particle sizes were
259 obtained by DLS (M2-A, M3-A, M5-A and M6-A), except for samples M1-A and M4-A which presented
260 large particles and no particles, respectively. It is important to point out that M1, M4 and M6 represent
261 the formulations with lower water content compared to the other systems. When M2-A, M3-A, M5-A
262 and M6-A samples were analyzed by SEM, all of them showed a spherical shape, although some
263 agglomerates were observed in M2-A sample. However, the size was also measured with ImageJ
264 software for all formulations tested. A size range between 12 nm and 47 nm was obtained for M2-A
265 sample. For M3-A sample a size range between 27 nm and 74 nm was obtained. In spite of the higher
266 sizes than the previous ones, the particles presented less aggregates and a greater number of particles
267 was obtained. The same effect was observed with sample M5-A, where the amount of particles obtained
268 was also higher, and the size range varied from 24 nm to 51 nm. Finally, large spherical particles were
269 obtained for sample M6-A, in contrast with the small sizes expected with the DLS results: the size range
270 for the SNPs varied from 64 nm to 180 nm and some particle aggregates were observed, also indicating
271 in this case that the formulations that correspond to the stability region with less water content indicate
272 is not suitable to form uniform SNPs.

273 Taking into account these sizes obtained, it can be concluded that the best results were achieved when
274 an aqueous phase containing 1% (w/v) starch dissolved in Milli-Q water was used in combination with
275 a precipitant solution containing NaOH (12% (w/v) NaOH in ethanol). Low aspect ratio particles were
276 thus obtained (samples A). NaOH breaks the hydrogen bonds between water and starch, resulting in the
277 disruption of the existing molecular orders within the starch granules (Neelam, Vijay & Lalit, 2021),
278 thus improving starch solubility in water (Han & Lim, 2004).

279 At the same time, with these synthesis parameters, microemulsion systems M2, M3 and M5 showed the
280 smallest particle sizes. The size obtained by DLS was around 40 nm for the sample M2-A, with a PdI
281 of 0.81. This high value of the polydispersity index can be explained by the fact that particle size varied
282 over a fairly wide range as mentioned above (from 12 nm to 47 nm). This explains that the sample is
283 not monodisperse, but it rather presents great variety of sizes. The same happened with the other two
284 samples: size obtained by DLS was around 34 nm for sample M3-A, with a PdI of 0.77 but ranging from
285 27 nm to 74 nm; for sample M5-A, size obtained with DLS was around 36 nm with a PdI of 0.98 in an
286 interval from 24 nm to 51 nm. The micrographs in Figure 3 show that small particles predominated in
287 samples M3-A and M5-A, which is consistent with the data obtained by DLS where slightly smaller
288 particles were observed compared to sample M2-A.



289
290 *Figure 3. SEM micrographs for M2-A, M3-A and M5-A systems*
291

292 From Figure 3, it could be estimated that both the M2-A system, as well as the M3-A and M5-A systems
293 were optimal the formulations to obtain small, spherical and homogeneous SNPs by the microemulsion
294 method. Similar results were reported by other authors (Zhou, Luo & Fu, 2014) who suggested the use
295 of the ME method to obtain SNPs with good sphericity, small size and a narrow particle size distribution
296 to be used as drug delivery systems.

297 **3.1.2. SNPs production yield**

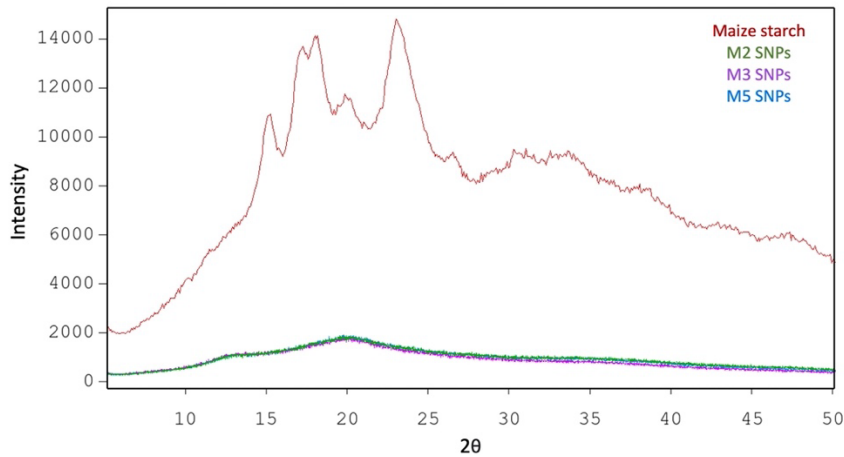
298 Once the synthesis conditions and the optimal microemulsion systems were selected, SNPs production
299 yield was determined. For this purpose, the total amount of SNPs per amount of starch added into the
300 aqueous phase was calculated. Samples were dried in a stove, in the same way as for the SEM
301 characterization, for 24 h at 80°C in small flat-bottomed glass tubes.

302 The experiments were carried out in triplicate and finally, for each 0.2 g of starch added to the aqueous
303 phase, 0.032 g of particles were obtained for the M2 microemulsion system, 0.020 g for the M3 system
304 and 0.029 g for the M5 system. The production yield of SNPs obtained was 16% for the M2 system,
305 10% for the M3 system and 15% for the M5 system.

306 **3.1.3. XRPD analysis**

307 XRPD was applied to determine the crystalline structure of starch granules as well as that of the SNPs
308 of the optimal formulations. The spectra are shown in Figure 4. Starch granules showed peaks at Bragg
309 angles (2θ) at 15°, 17°, 18° and 23° corresponding to A-type X-ray diffraction patterns, which is in good

310 agreement with results from previous studies (Lin et al, 2020).
311 Nevertheless, these starch characteristic peaks did not appear in the spectra obtained for the SNPs. This
312 may indicate that the synthesis process affected the crystalline structure of the starch granules, and
313 finally all synthesized SNPs showed an amorphous crystalline structure, which is in agreement with the
314 results obtained by other authors (Ding, Lin & Kan, 2018).



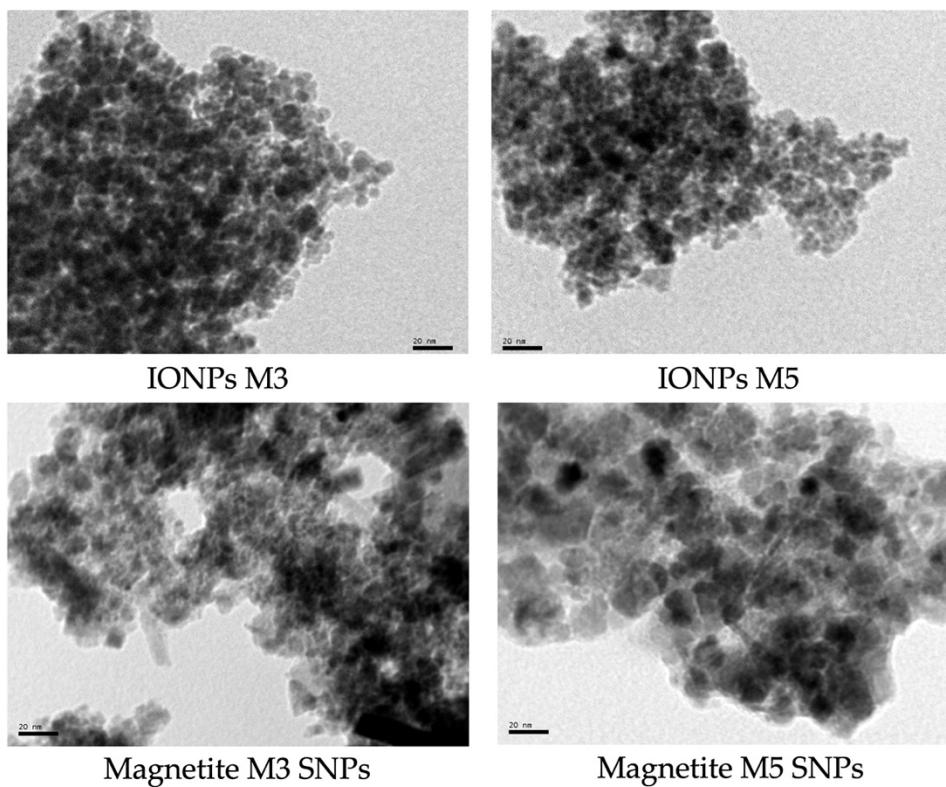
315
316 *Figure 4. XRPD spectra of starch granules and the resulting SNPs synthesized with the optimal*
317 *formulations.*

318
319 Dufresne et al summarized the polymer nanocomposite trend as a function of the nature (crystalline or
320 amorphous) of the matrix and its interaction with nanostructured fillers where several nanocomposites
321 presented amorphous structure with good interaction for different fillers. (Dufresne, Medeiros, &
322 William, 2009)

323 **3.2. Starch superparamagnetic nanocomposites (SNP-IONPs)**

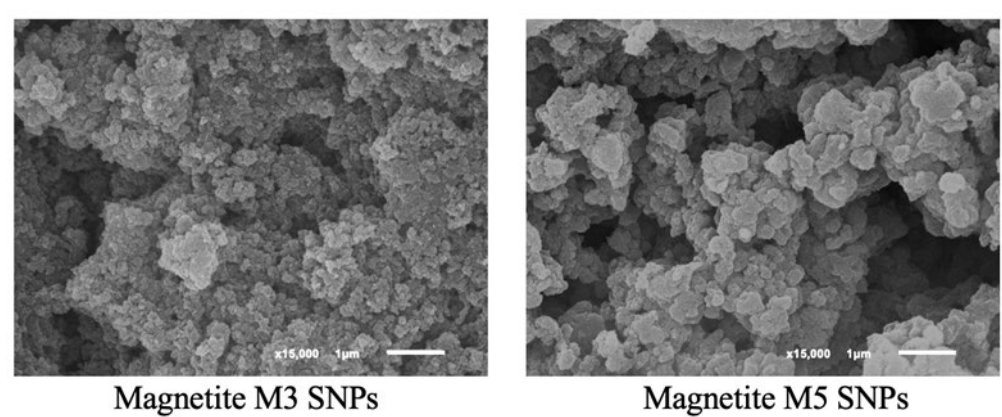
324 Formulations M3 and M5 were used to simultaneously synthesized SNPs and IONPs and produce size-
325 tuned starch-based superparamagnetic nanocomposites susceptible to be used for further
326 bioapplications. It has been demonstrated in previous studies that starch-based magnetic nanocapsules
327 have a major potential for the targeted delivery of hydrophilic bioactives through a magnetic field-
328 generated (Sousa et al, 2021). Similar trend was observed in another study where an effectively delivery
329 of the antitumor drug cisplatin from superparamagnetic nanoparticles of crosslinked starch impregnated
330 was reported in the presence and absence of magnetic field via diffusion-controlled pathway (Likhitar &
331 Bajpai, 2012).

332 Best results for the synthesized nanoparticles were obtained for these M3 and M5 systems with a size
333 range that varied between sizes from 28 nm to 55 nm for system M3, and between 23 nm y 73 nm for
334 system M5. The average diameters varied between 44 nm and 43 nm respectively. TEM micrographs
335 shown in Figure 5 revealed the formation of low aspect ratio particles despite of certain agglomeration
336 degree and some irregular shapes. In both micrographs, the SNPs with IONPs can be easily identified.
337 In turn, the properties of these SNP-IONPs composited can be compared with those of the iron salts in
338 absence of starch (IONPs M3 and IONPs M5).



339
 340 *Figure 5. TEM micrographs of the superparamagnetic SNPs and IONPs obtained with M3 and M5*
 341 *microemulsion systems.*
 342

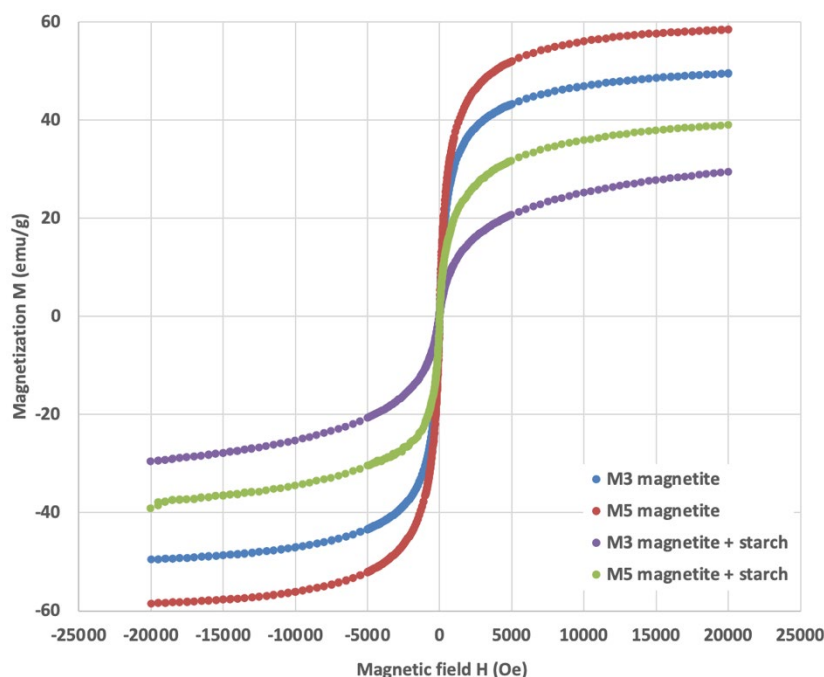
343 In addition, Figure 6 shows the SEM micrographs where the different particle sizes for each system can
 344 be seen.



345
 346 *Figure 6. SEM micrographs of the superparamagnetic SNPs (SNP-IONPs composites) obtained with*
 347 *M3 and M5 microemulsion systems.*
 348

349 At the same time, magnetization studies with iron oxide SNPs were performed and compared with
 350 IONPs synthesized in absence of starch (named as magnetite samples M3 and M5). Rebodos &
 351 Vikesland, reported that, based on magnetisation loops, magnetite nanoparticles exhibited
 352 superparamagnetic-like behaviour, which was expected for particles within a small size range (Rebodos
 353 & Vikesland, 2010).

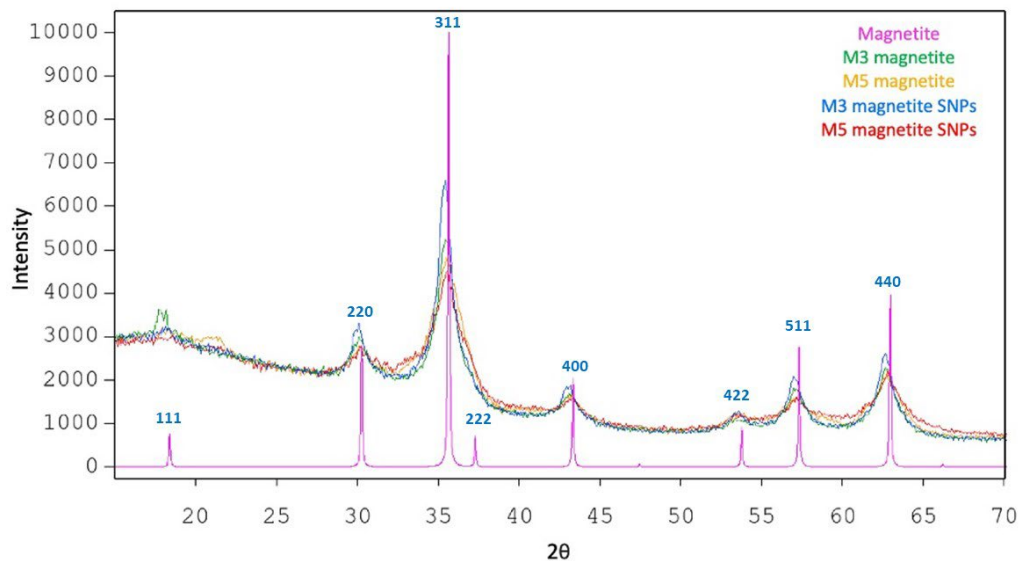
354 Figure 7 shows the magnetization (M) versus the applied magnetic field (H) curve obtained at room
355 temperature curves for SNPs-IONPs composites (M3 magnetite + starch and M5 magnetite + starch
356 samples) and the corresponding bare IONPs in absence of starch (M3 magnetite and M5 magnetite
357 samples). The absence of hysteresis loop confirms the superparamagnetic behaviour of all samples
358 analysed. The saturation magnetization of magnetite nanoparticles has been determined by setting the
359 experimental data to the law of approach to saturation (Zhang, Zeng & Liu, 2010) and their values were
360 49.5 emu/g for M3 sample and 58.5 emu/g for M5 sample, being similar to those reported in a previous
361 study where IONPs were synthesized by the ME method (Salvador et al., 2021). Similar results were
362 also reported by Likhitar & Bajpai who obtained a saturation magnetization of about 58 emu/g (Likhitar
363 & Bajpai, 2012). However, it was noticed that, for both formulations, the iron oxide impregnated SNPs
364 showed lower magnetization and superparamagnetic behaviour properties than their corresponding bare
365 IONPs. This can be explained by the fact that IONPs are impregnated in a starch matrix consisting of
366 SNPs.



367
368 *Figure 7. Magnetization curves for SNPs-IONPs composites and the corresponding bare IONPs in*
369 *absence of starch.*
370

371 Finally, XRPD diagrams were collected to compare the obtained nanocrystalline phases with the
372 magnetite reference structure (Nakagiri, Manghnani, Ming & Kimura, 1986) since XRPD analysis is an
373 important tool for determination of crystallinity of materials (Gupta & Bajpai, 2010) and has also been
374 used for previous authors to demonstrate the presence of iron oxide nanoparticles in superparamagnetic
375 nanoparticles of crosslinked starch impregnated designed for drug delivery purposes (Likhitar & Bajpai,
376 2012). The spectra are shown in Figure 8. In all the XRPD diagrams the corresponding peaks match the
377 spectral pattern of the pure magnetite structure, named in the diagram as magnetite sample, which means

378 that pure crystalline phases have been obtained in this work.



379
380 *Figure 8. XRPD spectra of IONPs (M3 and M5 magnetite) and SNPs-IONPs (M3 magnetite SNPs and*
381 *M5 magnetite SNPs) for M3 and M5 systems.*

383 4. Conclusions

384 The synthesis of size-tuned SNPs (30-40 nm) was achieved through the use of a microemulsion method.
385 This was possible by controlling the ratio and composition of the reagents used in the microemulsion
386 system (aqueous and organic phases, stabilizer and co-stabilizer), as well as the precipitating agents
387 used.

388 Moreover, the versatility of the developed ME method has also been demonstrated, as iron oxide SNPs
389 with controlled size and superparamagnetic properties were also synthesized simultaneously using this
390 method what validates the hypothesis stated and confirms the potential of this method as an innovative
391 technology for the design and development of new functional nanomaterials.

392 The synthesized size-tuned magnetic-polymeric nanocomposites are promising materials that are likely
393 to be used for different biomedical applications, such as drug delivery nanocarriers or potential markers
394 for theragnostic purposes.

395 CRediT authorship contribution statement

396 **D. Morán:** Conceptualization, Validation, Formal analysis, Resources, Data curation, Writing - original
397 draft. **G. Gutiérrez:** Conceptualization, Validation, Writing - review & editing, Supervision, Project
398 administration. **M. Rayner:** Conceptualization, Validation. **C. Blanco-López:** Conceptualization,
399 Validation, Funding acquisition. **R. Mendoza:** Conceptualization, Validation, Formal analysis. **M.**
400 **Matos:** Conceptualization, Validation, Writing - review & editing, Supervision, Project administration.

401 402 Acknowledgements

403 This work was supported by Ministerio de Economía y Empresa (MINECO, Spain) under Grant
404 MAT2017-84959-C2-1-R, PID2020-119087RB-I00, PDC2021-121444-I00 and RED2018-102626-T.
405 This study was also cofinanced by Consejería de Educación y Ciencia del Principado de Asturias
406 (AYUD/2021/52132). Authors would like to acknowledge the technical support provided by Servicios
407 Científico-Técnicos de la Universidad de Oviedo.

408

409 **5. References**

410 Asgari, S., Saberi, A.H., McClements, D.J., & Lin, M. (2019). Microemulsions as nanoreactors for
411 synthesis of biopolymer nanoparticles. *Trends in Food Science & Technology*, *86*, 118–130. doi:
412 10.1016/J.TIFS.2019.02.008.

413 Chin, S.F., Azman, A., & Pang, S.C. (2014). Size Controlled Synthesis of Starch Nanoparticles by a
414 Microemulsion Method. *Journal of Nanomaterials*, *ID763736*. doi: 10.1155/2014/763736.

415 Chin, S.F., Pang, S.C., & Tay, S.H. (2011). Size controlled synthesis of starch nanoparticles by a simple
416 nanoprecipitation Method. *Carbohydrate Polymers*, *86*, 1817–1819. doi:
417 10.1016/j.carbpol.2011.07.012.

418 Darroudi, M., Hakimi, M., Goodarzi, E., & Kazemi Oskuee R. (2014). Superparamagnetic iron oxide
419 nanoparticles (SPIONs): Green preparation, characterization and their cytotoxicity effects. *Ceramics*
420 *International*, *40*, 9, 14641–14645. doi: 10.1016/J.CERAMINT.2014.06.051.

421 Ding, Y., Lin, Q., & Kan, J. (2018). Development and characteristics nanoscale retrograded starch as an
422 encapsulating agent for colon-specific drug delivery. *Colloids and Surfaces B: Biointerfaces*, *171*, 656-
423 667. doi: 10.1016/j.colsurfb.2018.08.007.

424 Dufresne, A., Medeiros, E., & William, J. (2009). Starch-based Nanocomposites. (Chapter 9)

425 Gupta, R., & Bajpai, A. K. (2010). Magnetically guided release of ciprofloxacin from superparamagnetic
426 polymer nanocomposites. *Journal of Biomaterial Science*, *26*, 1–26. doi:10.1016/j.carbpol.2011.07.053.

427 Gutiérrez, G., Morán, D., Marefati, A., Puhagen, J., Rayner, M., & Matos, M. (2020). Synthesis of
428 controlled size starch nanoparticles (SNPs). *Carbohydrate Polymers*, *250*, 116938. doi:
429 10.1016/j.carbpol.2020.116938.

430 Han, J.A., & Lim, S.T. (2004). Structural changes in corn starches during alkaline dissolution by
431 vortexing. *Carbohydrate Polymers*, *55*(2), 193-199. doi: 10.1016/j.carbpol.2003.09.006.

432 Kim, H.Y., Park, S.S., & Lim, S.T. (2015). Preparation, characterization and utilization of starch
433 nanoparticles. *Colloids and Surfaces B: Biointerfaces*, *126*, 607–620. doi:

434 10.1016/j.colsurfb.2014.11.011.

435 Le Corre, D., Bras, J. & Dufresne, A. (2010). Starch Nanoparticles: A Review. *Biomacromolecules*, *11*,
436 1139–1153. doi: 10.1021/bm901428y.

437 Likhitkar, S., & Bajpai, A.K. (2012). Magnetically controlled release of cisplatin from
438 superparamagnetic starch nanoparticles. *Carbohydrate Polymers*, *87*, 1, 300-308. doi:
439 10.1016/j.carbpol.2011.07.053.

440 Lin, Q., Ji, N., Li, M., Dai, L., Xu, X., Xiong, L., & Sun, Q. (2020). Fabrication of debranched starch
441 nanoparticles via reverse emulsification for improvement of functional properties of corn starch films.
442 *Food Hydrocolloids*, *104*, 105760. doi: 10.1016/j.foodhyd.2020.105760.

443 Liu, C., Li, K., Li, X., Zhang, M., & Li, J. (2021). Formation and structural evolution of starch
444 nanocrystals from waxy maize starch and waxy potato starch. *International Journal of Biological*
445 *Macromolecules*, *180*, 625–632. doi: 10.1016/J.IJBIOMAC.2021.03.115.

446 Malhotra, N., Lee, J.S., Liman, R.A.D., Ruallo, J.M.S., Villaflores, O.B., Ger, T.R., & Hsiao, C.D.
447 (2020). Potential Toxicity of Iron Oxide Magnetic Nanoparticles: A Review. *Molecules*, *25*(14), 3159.
448 doi: 10.3390/molecules25143159.

449 Materón, E.M., Miyazaki, C.M., Carr, O., Joshi, N., Picciani, P.H.S., Dalmaschio, C.J., Davis, F., &
450 Shimizu, F.M. (2021). Magnetic nanoparticles in biomedical applications: A review. *Applied Surface*
451 *Science Advances*, *6*, 100163. doi: 10.1016/j.apsadv.2021.100163.

452 Medeiros, S.F., Filizzola, J.O.C., Fonseca, V.F.M., Oliveira, P.F.M., Silva, T.M., Elaissari, A., & Santos,
453 A.M. (2015). Synthesis and characterization of stable aqueous dispersion of functionalized double-
454 coated iron oxide nanoparticles. *Materials Letters*, *160*, 522-525. doi: 10.1016/j.matlet.2015.08.026.

455 Morán, D., Gutiérrez, G., Blanco-López, M.C., Marefati, A., Rayner, M., & Matos, M. (2021). Synthesis
456 of starch nanoparticles and their applications for bioactive compound encapsulation. *Applied Sciences*,
457 *11*, 4547. doi:10.3390/app11104547.

458 Najafi, S.H.M., Baghaie, M., & Ashori, A. (2016). Preparation and characterization of acetylated starch
459 nanoparticles as drug carrier: Ciprofloxacin as a model. *International Journal of Biological*
460 *Macromolecules*, *87*, 48–54. doi: 10.1016/j.ijbiomac.2016.02.030.

461 Nakagiri, N., Manghnani, M.H., Ming, L.C., & Kimura, S. (1986). Crystal structure of magnetite under
462 pressure. *Physics and Chemistry of Minerals*, *13*, 238-244. doi: 10.1007/BF00308275.

463 Neelam, K., Vijay, S., & Lalit, S. (2012). VARIOUS TECHNIQUES FOR THE MODIFICATION OF

464 STARCH AND THE APPLICATIONS OF ITS DERIVATIVES Kaviani. *International Research*
465 *Journal of Pharmacy*, 3 (5).

466 Rebodos, R.L., & Vikesland, P.J. (2010). Effects of Oxidation on the Magnetization of Nanoparticulate
467 Magnetite. *Langmuir*, 26, 22, 16745–16753. doi:10.1021/la102461z.

468 Saari, H., Fuentes, C., Sjöo, M., Rayner, M., & Wahlgren, M. (2017). Production of starch nanoparticles
469 by dissolution and non-solvent precipitation for use in food-grade Pickering emulsions. *Carbohydrate*
470 *Polymers*, 157, 558-566. doi: 10.1016/J.CARBPOL.2016.10.003.

471 Salvador, M., Gutiérrez, G., Noriega, S., Moyano, A., Blanco-López, M.C., & Matos, M. (2021).
472 Microemulsion Synthesis of Superparamagnetic Nanoparticles for Bioapplications. *International*
473 *Journal of Molecular Sciences*, 22(1), 427. doi: 10.3390/ijms22010427.

474 Soares, P.I.P., Laia, C.A.T., Carvalho, A., Pereira, L.C.J., Coutinho, J.T., Ferreira, I.M.M., Novo,
475 C.M.M., & Borges, J.P. (2016). Iron oxide nanoparticles stabilized with a bilayer of oleic acid for
476 magnetic hyperthermia and MRI applications. *Applied Surface Science*, 383, 240-247. doi:
477 10.1016/j.apsusc.2016.04.181.

478 Sousa, A., Romo, A., Almeida, R., Silva, A., Fechine, L., Brito, D., Freire, R., Pinheiro, D., Silva, L.,
479 Pessoa, O., Denardin, J., Pessoa, C., & Ricardo, N. (2021). Starch-based magnetic nanocomposite for
480 targeted delivery of hydrophilic bioactives as anticancer strategy. *Carbohydrate Polymers*, 264, 118017.
481 doi: 10.1016/j.carbpol.2021.118017.

482 Vaghari, H., Jafarizadeh-Malmiri, H., Mohammadlou, M., Berenjian, A., Anarjan, N., Jafari, N., &
483 Nasiri, S. (2016). Application of magnetic nanoparticles in smart enzyme immobilization. *Biotechnology*
484 *Letters* 38, 223–233. doi: 10.1007/s10529-015-1977-z

485 Valdiglesias, V., Fernández-Bertólez, N., Kiliç, G., Costa, C., Costa, S., Fraga, S., Bessa, M.J., Pásaro,
486 E., Teixeira, J.P., & Laffon, B. (2016). Are iron oxide nanoparticles safe? Current knowledge and future
487 perspectives. *Journal of Trace Elements in Medicine and Biology*, 38, 53-63. doi:
488 10.1016/j.jtemb.2016.03.017.

489 Wang, X., Chen, H., Luo, Z., & Fu, X. (2016). Preparation of starch nanoparticles in water in oil
490 microemulsion system and their drug delivery properties. *Carbohydrate Polymers*, 138, 192–200. doi:
491 10.1016/J.CARBPOL.2015.11.006.

492 Zhang, H., Zeng, D., & Liu, Z. (2010). The law of approach to saturation in ferromagnets originating
493 from the magnetocrystalline anisotropy. *Journal of Magnetism and Magnetic Materials*, 322, 16, 2375-
494 2380. doi:10.1016/j.jmmm.2010.02.040.

495 Zhou, P., Luo, Z., & Fu, X. (2014). Preparation and characterization of starch nanoparticles in ionic
496 liquid-in-oil microemulsions system. *Industrial Crops and Products*, 52, 105-110.
497 doi:10.1016/j.indcrop.2013.10.019.